Volume 20
Number 18
14 May 2024
Pages 3711–3878

Soft Matter

rsc.li/soft-matter-journal

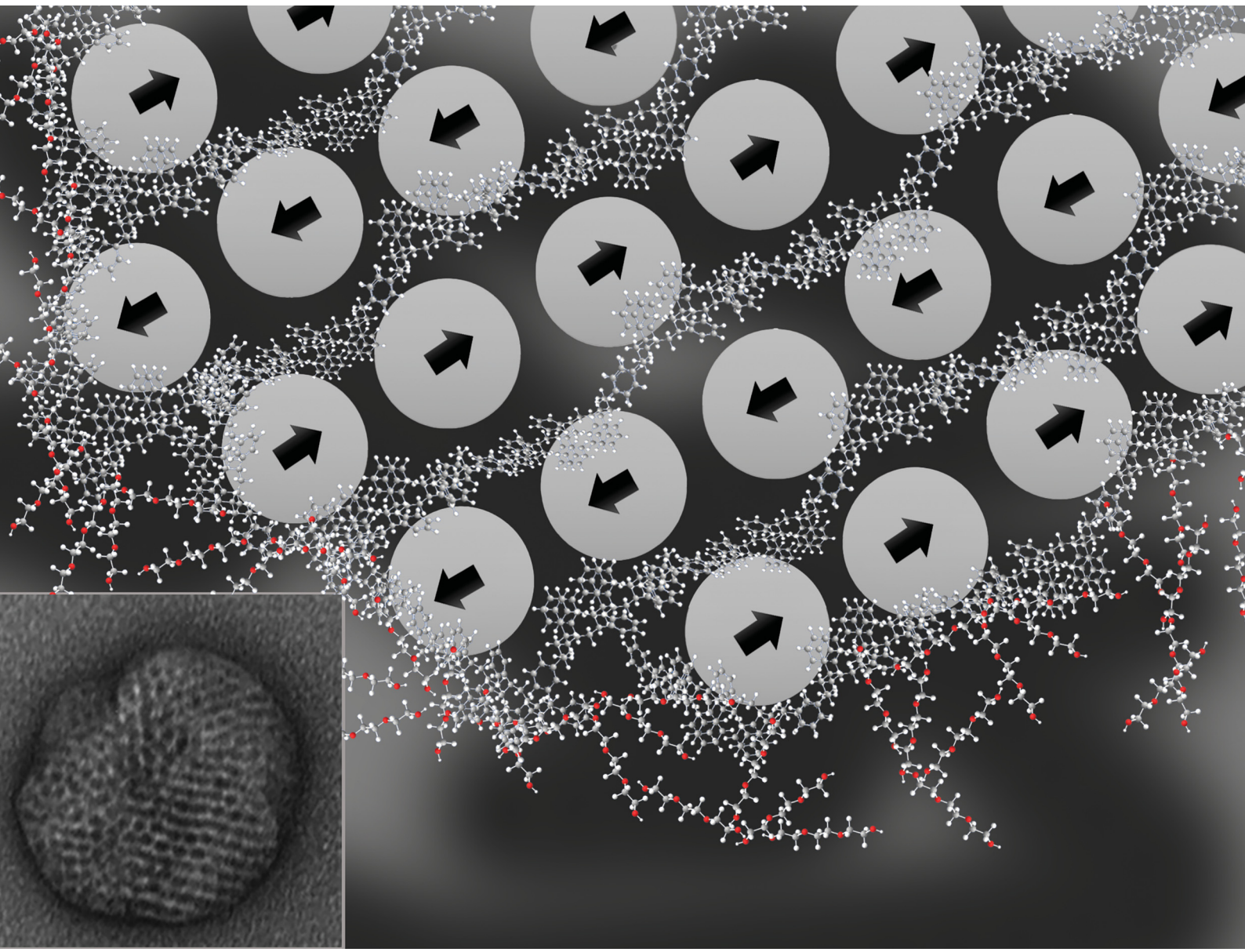

ISSN 1744-6848

ROYAL SOCIETY OF CHEMISTRY

PAPER
Jessica O. Winter *et al.*
Structural interactions in polymer-stabilized magnetic nanocomposites

Soft Matter

PAPER

View Article Online
View Journal | View Issue

Cite this: *Soft Matter*, 2024, **20**, 3732

Structural interactions in polymer-stabilized magnetic nanocomposites†‡

Gauri M. Nabar,§[a] Abhilasha V. Dehankar, §[a] Elizabeth Jergens, [a] Benworth B. Hansen, [a] Ezekiel Johnston-Halperin, [b] Matthew Sheffield, [b] Joshua Sangoro, [a] Barbara E. Wyslouzil [ac] and Jessica O. Winter *[ad]

Superparamagnetic iron oxide nanoparticles (SPIONs) have attracted significant attention because of their nanoscale magnetic properties. SPION aggregates may afford emergent properties, resulting from dipole–dipole interactions between neighbors. Such aggregates can display internal order, with high packing fractions (>20%), and can be stabilized with block co-polymers (BCPs), permitting design of tunable composites for potential nanomedicine, data storage, and electronic sensing applications. Despite the routine use of magnetic fields for aggregate actuation, the impact of those fields on polymer structure, SPION ordering, and magnetic properties is not fully understood. Here, we report that external magnetic fields can induce ordering in SPION aggregates that affect their structure, inter-SPION distance, magnetic properties, and composite T_g. SPION aggregates were synthesized in the presence or absence of magnetic fields or exposed to magnetic fields post-synthesis. They were characterized using transmission electron microscopy (TEM), small angle X-ray scattering (SAXS), superconducting quantum interference device (SQUID) analysis, and differential scanning calorimetry (DSC). SPION aggregate properties depended on the timing of field application. Magnetic field application during synthesis encouraged preservation of SPION chain aggregates stabilized by polymer coatings even after removal of the field, whereas post synthesis application triggered subtle internal reordering, as indicated by increased blocking temperature (T_B), that was not observed *via* SAXS or TEM. These results suggest that magnetic fields are a simple, yet powerful tool to tailor the structure, ordering, and magnetic properties of polymer-stabilized SPION nanocomposites.

Received 3rd January 2024,
Accepted 12th April 2024

DOI: 10.1039/d4sm00008k

rsc.li/soft-matter-journal

Introduction

The assembly of inorganic nanoparticles (NPs) into well-ordered superstructures is crucial for harnessing their unique properties to practical applications in optics, electronics, biosensing, data storage, and energy harvesting.[2] In addition to their individual properties, spatially interacting inorganic NPs can demonstrate emergent, collective behaviours when ordered into composites.[3–6] For example, simultaneous excitation of gold NPs in arrays or superlattices enhances their electromagnetic fields through plasmonic interactions.[7,8] As a result, a variety of 2D and 3D NP superstructures have been developed and investigated.[3–6,9–11] One composition of particular interest is the assembly of superparamagnetic iron oxide NPs (SPIONs) into 2D and 3D arrays. In the presence of magnetic fields, dispersed SPIONs can align in the direction of the magnetic field. Upon field removal and provided sufficient separation distance, SPIONs relax to their equilibrium states independent of the orientation of other SPIONs in the system. However, when SPIONs are in close proximity, as might be expected in a superlattice, their orientations after magnetic field removal may be strongly influenced by those of neighbouring SPIONs as a result of distance-dependent dipole coupling.[12,13] Thus, the magnetic properties of SPION aggregates can depend on the aggregate structure.

Such aggregates can be generated through a variety of methods, including DNA origami for precision placement[14–16] or less ordered structures through colloidal self-assembly.[17,18] Colloidal aggregates are an attractive choice because of their ease of synthesis. The structure of these colloidal aggregates is primarily determined by the effective interaction potential resulting from the cumulative fundamental attraction and

[a] *William G. Lowrie Department of Chemical and Biomolecular Engineering, The Ohio State University, 151 W. Woodruff Ave., Columbus, OH 43210, USA. E-mail: winter.63@osu.edu*
[b] *Department of Physics, The Ohio State University, Columbus, Ohio 43210, USA*
[c] *Department of Chemistry and Biochemistry, The Ohio State University, 151 W. Woodruff Ave., Columbus, OH 43210, USA*
[d] *Department of Biomedical Engineering, The Ohio State University, 151 W. Woodruff Ave., Columbus, OH 43210, USA*

† Portions of this material were published in the PhD thesis of GMN[36] and are cited where appropriate.

‡ Electronic supplementary information (ESI) available. See DOI: https://doi.org/10.1039/d4sm00008k

§ Gauri M. Nabar and Abhilasha V. Dehankar contributed equally to this work.

repulsion forces between SPIONs, such as van der Waals, steric, magnetic dipole, and electrostatic forces from attached ligands. Such forces can be leveraged to alter not only the final structure, but also any metastable structures that form during synthesis. For example, magnetic fields applied during synthesis may induce structural transformations that effect ordering in the final material, altering the collective magnetism of the aggregate. A deeper understanding of these magnetically induced structural transformations could provide opportunities to tailor 3D SPION aggregate properties through external magnetic field application. Most previous studies of SPION colloidal clusters have focused on tuning their magnetic properties through synthesis methods.[4,19–22] The influence of magnetic fields applied during and post-synthesis on structural ordering has yet to be explored. Also, few of these studies examined the influence of nanoparticle magnetic ordering on the properties of the polymers used to stabilize these aggregates.

Our group has established a new route to NP aggregates *via* self-assembly assisted by polystyrene (PS)-*b*-polyethylene oxide (PEO) block copolymers (BCPs). Densely loaded aggregates formed that consist of NP aggregates coated by amphiphilic BCPs rendering them soluble in aqueous media. These structures exhibit high NP volume concentration (up to 24%) with semi-ordered packing and NP separation distances smaller than NP diameters (*e.g.*, ~2 nm edge-to-edge for ~6 nm NPs).[23] These loadings are well above those of commercial magnetic particles used for cell separation, which have magnetic NP packings between 5–10%.[24] For example, an 80 nm diameter, densely loaded aggregate can contain up to 900 encapsulated SPIONs, making this vehicle an ideal model system for evaluating the effect of magnetic fields on emergent SPION aggregate properties and 3D superlattice formation.

Here, we leveraged the high packing volume and low inter-NP spacing of these densely loaded SPION aggregates to assess the impact of magnetic field application during and after synthesis on emergent structural and magnetic properties of SPION clusters. Nanoscale aggregate morphology was evaluated using transmission electron microscopy (TEM) and image analysis. NP packing was examined using complementary small angle X-ray scattering (SAXS) measurements of aggregate solutions. Magnetic properties, specifically coercivity and blocking temperatures, were measured using a superconducting quantum interference device (SQUID). Changes in stabilizing polymer properties, specifically T_g, were measured using differential scanning calorimetry (DSC). Morphology and changes in polymer and magnetic properties were used to establish structure–property relationships for densely loaded aggregates with differing SPION orientations, including structural and magnetic ordering induced by external magnetic fields. This work presents an investigation of magnetically induced ordering in densely loaded SPION aggregates. Such composites offer promise for applications requiring tailored magnetic ordering and fields, including magnetic resonance imaging, cell separations, and magnetic storage.

Experimental

Materials

Carboxyl-terminated poly(styrene-*block*-ethylene oxide, PS90-*b*-PEO400) (Cat no. P5755-SEOCOOH) was purchased from Polymer Source Inc. (Montreal, Canada). Poly(vinyl alcohol) (PVA) (Cat no. 363170) was purchased from Sigma Aldrich. Chloroform (Cat no. C606SK-4) was purchased from Fisher Scientific. Oleic-acid coated SPIONs (5 nm diameter, Cat no. SOR-05-50) in chloroform were purchased from Ocean NanoTech, CA. All materials were used as received without further purification.

Methods

SPION nanocomposite formation with and without magnetic field application. Several different nanocomposites and controls were investigated (Fig. 1). SPION nanocomposites were prepared in the absence of a magnetic field using the interfacial instability method[25,26] described previously.[23] These samples will be denoted by SNC throughout the remainder of the paper. Briefly, an organic phase consisting of SPIONs and PS-*b*-PEO in a 1 : 1 mole ratio was prepared by combining 100 μL of PS-*b*-PEO (1 mg mL^{-1} in chloroform) with 211 μL of SPIONs (2.5 mg mL^{-1} in chloroform). An emulsion was formed by mixing the organic phase with PVA (3 mL, 5 mg mL^{-1} in water) and sonicated (Cole-Parmer SS Ultrasonic Cleaner, Heater/Digital Timer; 3.5 gal, 220 V #item number EW-08895-58) at 20 °C for one hour in fresh, cold tap water. Here, PVA is used as a surfactant to control droplet size and provide the transiently negative surface tension needed for droplet ejection in the interfacial instability technique. Then, the sonicated emulsion was placed in an aluminium dish (internal diameter = 5 cm) on a rocker for 2.5 hours to evaporate residual chloroform. Successful SNC formation was indicated by a change in the initial cloudy solution with visible emulsion droplets to a clear, brown solution.

SPION nanocomposites formed in the presence of a magnetic field will be referred to as magnetically stirred SNC or denoted by SNC-St. To produce the SNC-St, an emulsion was initially generated by manual shaking in a glass vial (internal diameter = 2.3 cm) and then stirred at 60 rpm using a magnetic stir bar (Alnico, forged steel, Fig. S1, ESI‡) with a maximum

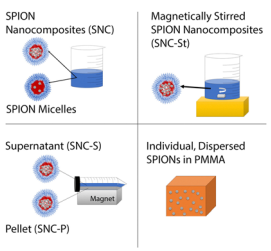

Fig. 1 Schematics of different nanocomposites and controls investigated. SPION nanocomposites (SNC) and SPION micelles were formed in the absence of magnetic fields, whereas magnetically stirred aggregates (SNC-St) were formed under magnetic stirring. SNC samples exposed to a magnet after synthesis yielded a magnetically collected pellet (SNC-P) and the supernatant (SNC-S). Individual SPIONs dispersed in PMMA polymer comprised the control.

magnetic flux density of 60 Oe under atmospheric conditions for 12 hours.

In both synthesis methods, unencapsulated SPIONs were eliminated by centrifugation at 4000 rcf for 1 minute. Because of the mechanism involved, the interfacial instability method yields samples that contain densely loaded aggregates,[23] micelles incorporating SPIONs (*i.e.*, SPION-micelles) and SPION free micelles (*i.e.*, empty micelles). In densely loaded aggregates a cluster containing many SPIONs occupies the central volume of the micelle, whereas SPION-micelles exhibit a void volume with a low number of encapsulated SPIONs. Clusters were classified in TEM images using these characteristics.

Magnetic field applied to SNC samples post-synthesis. To evaluate the effect of magnetic field application post-synthesis, 1 mL of SPION nanocomposite samples were transferred into 1.5 mL centrifuge tubes and exposed to a 0.5 T magnet for 9 hours by holding the entire length of the centrifuge tube up to the magnet surface. After exposure, a brown pellet collected near the magnet surface, but the supernatant did not become clear, consistent with particles also remaining dispersed in the solution. The pellet was collected, and this sample will be referred to as SNC-P (Fig. 1). The remaining supernatant will be referred to as SNC-S. These samples were subjected to further analysis *via* TEM, SAXS, SQUID, and DSC.

Transmission electron microscopy (TEM). All SNC samples were imaged *via* TEM using an FEI Tecnai G2 Bio Twin. Prior to imaging, samples were negatively stained using uranyl acetate (UA, 1 wt%) to increase contrast. Samples (10 μL) were deposited on silicon pads and formvar/carbon-coated nickel TEM grids were placed on these droplets, carbon side down, for two minutes. Sample not deposited was removed using filter paper; then, UA stain (10 μL) was applied for 60 seconds, and excess removed using filter paper. Grids were air dried, carbon-side up. For each sample, between 100 to 1000 individual particles were imaged and analysed. Analysis of size and aspect ratio was obtained using NIH ImageJ[27] software with the 'analyse particles' feature and the 'measure ROI curve plugin'. Particles were characterized as empty micelles if no SPIONs were visible, SPION micelles if they were similar to empty micelles in size and interiors were not completely filled with NPs, and densely loaded aggregates (SNC) if they were larger than empty micelles and displayed complete or near complete filling of the interior (Fig. S2, ESI‡).

Small angle X-ray scattering (SAXS). SAXS measurements were conducted at Argonne National Labs Advanced Photon Source, (Argonne, IL) using the 12-ID-C beamline. The incident X-ray wavelength was 0.1 nm[1] and the scattering wavevector range was $0.005\ \text{Å}^{-1} < Q < 0.6\ \text{Å}^{-1}$. Samples were evaluated at a low PS-*b*-PEO concentration of 0.001 wt%. Thus, the background subtracted signal was mainly derived from electron dense SPIONs in the composite.

Superconducting quantum interference device (SQUID) magnetometer. Magnetic measurements were conducted on SNC samples sealed in EPR tubes using a Quantum Designs MPMS XL. Isothermal magnetization measurements were performed by scanning $-10\ \text{kOe} \leq$ applied magnetic field ≤ 10 kOe. Sample temperature dependence was studied by measuring field-cooled (FC) and zero field-cooled (ZFC) curves by cooling the samples from 300 K to 2 K at 5 T and at zero applied field, respectively, and recording magnetic response while warming from 2 K to 300 K under a low applied field of 50 Oe. Magnetic properties of individual SPIONs were measured by dispersing organic SPIONs in a polymethylmethacrylate (PMMA) polymer matrix at low concentration (1.25% w/w). Results are reported and compared after normalization. The normalized standard deviation in the measurement fit of each sample for different types of magnetic measurements are reported in Table S1 (ESI‡).

Differential scanning calorimetry (DSC). DSC measurements were performed on a TA Instruments DSC 2500 unit. SNC samples were loaded into hermetically sealed TZero DSC pans to ensure that zero mass transfer with the environment occurred. Samples were annealed at 120 °C for a minimum of 10 minutes to erase thermal histories; then, the samples were cycled several times between 120 and −120 °C at a ramp rate of at 2 °C min^{-1} to verify repeatability of signals. Glass transition signals (T_g) were identified as the midpoint of the observed 2nd order thermal transitions, with errors within plus/minus 2 °C.

Results and discussion

SNC containing densely loaded aggregates in the absence of external magnetic fields

SNC containing densely loaded aggregates were assembled using the interfacial instability method introduced by Hayward.[26] In this approach, organic-soluble NPs are mixed with stabilizing amphiphilic BCPs and emulsified in the presence of surfactant. In the interfacial instability method, a large excess of surfactant relative to BCP (up to 100 : 1 weight ratio) is employed. Nanocomposites form upon evaporation of the organic solvent aided by droplet fission resulting from surface tension instabilities. At 1 : 1 NP : polymer molar ratios,[23] this approach yields densely loaded aggregates as well as NP-loaded micelles and empty micelles not containing NPs. Synthesis of densely loaded aggregates is believed to proceed first by NP aggregation, followed by polymer coating of the aggregate surface.[21] Thus, BCP chains are likely interacting with the surface of the NP aggregate, as well as intercalating with selected NPs. In contrast, micelle formation occurs when NP aggregation times are equal to or slower than those for BCP aggregation, resulting in encapsulation of a small number of dispersed NPs within the micelle hydrophobic matrix. In this case, the micelle core is composed primarily of the BCP hydrophobic block. Empty micelles are generated if BCPs aggregate in the absence of NPs, and indicate poor mixing conditions with concentration inhomogeneities. Empty micelle production can be minimized using high throughout reactors with high mixing intensity.[28]

We first evaluated SNCs produced at a 1 : 1 NP : polymer molar ratio in the absence of magnetic fields. Under these conditions, both densely loaded aggregates (8.5% by number)

Table 1 Size (mean ± standard deviation) and distribution of densely loaded aggregates (aggregates) and empty- or SPION-micelles (micelles) under different magnetic field application conditions

Sample	N^a	Aggregates[b] (nm) (%)	Micelles (nm) (%)
SNC	779	62.4 ± 27.0	25.6 ± 8.0
		8.5	91.5
SNC-St	345	107.0 ± 39.0	32.4 ± 8.0
		24.2	75.8
SNC-P	352	50.2 ± 21.0	26.2 ± 8.0
		39.5	60.5
SNC-S	1192	54.6 ± 22.0	23.2 ± 8.8
		8.1	91.9

[a] Number of particles analysed. [b] Percent by number of nanocomposites classified as aggregates or micelles.

and micelles (with or without SPIONs) (91.5%) were observed (Table 1). Densely loaded aggregate populations displayed average diameters of 62.4 ± 27.0 nm and log-normal size distribution; some internal NP ordering (*i.e.*, chaining) was also observed with centre to centre spacing of ~5.6 ± 0.94 nm (Fig. 2). In contrast, SPION-micelles displayed sizes of ~25.6 ± 8.0 nm with log normal size distribution and no observed NP ordering. NPs were not tightly packed and there were heterogeneities in NP distribution throughout the micelle. The sizes reported here for both populations were not statistically different from those we reported previously[23] (*i.e.*, $\alpha = 0.05$). The increased polydispersity of densely loaded aggregates compared to micelles could be explained by variation in aggregate nucleation and growth kinetics, which depends on uncontrolled factors in this system, such as local gradients in NP and polymer concentrations, interparticle distance in solution, and thermal fluctuations. The tight NP packing, as well as occasional chaining, observed within densely loaded aggregates, but not SPION micelles, is consistent with our previous small angle X-ray scattering (SAXS) analysis,[23,29] in which spectra could only be fit by including a hard sphere structure factor.

Effect of magnetic field exposure during SNC-St formation

To evaluate the role of magnetic field application during synthesis on the resulting aggregate morphology, SNC-St samples were produced by manual shaking followed by solvent evaporation under a continuously fluctuating magnetic field supplied by a magnetic stir bar ($0 \leq$ magnetic fields (Oe) ≤ 60) (Fig. S1, ESI‡). Interestingly, under magnetic field application the entire population of composites formed could be strictly divided into empty micelle (75.8%) and densely loaded aggregates (24.2%) (Table 1). In contrast to SNC samples, no SPION-micelles were observed. The densely loaded aggregates in the SNC-St samples were larger (107 ± 39 nm) than those in the SNC samples (62.4 ± 27.0 nm) and their size distribution was best described by a Gaussian function (Fig. 3). The size distribution of the entire SNC-St sample, however, maintained log-normal shape. Empty micelles displayed sizes of 32.4 ± 8.0 nm, similar to those observed in our previous paper[23] and to those reported by others.[25,30]

In addition to changes in overall composite size, we also observed striking changes to internal structure within the densely loaded aggregates. In the SNC-St samples, semi-periodic SPION arrays emerged (Fig. 4) that were not observed in the densely loaded aggregates found in the SNC samples (Fig. 2). Within a linear array, the centre-to-centre SPION distance is ~3.72 ± 0.61 nm, but spacing between linear arrays increases to ~7.29 ± 0.81 nm (two replicates, $N > 100$). This internal ordering indicates a transition to a more structured phase. Since TEM images are 2D projections of 3D objects, the radial organization of SPIONs within these structures cannot be fully evaluated. Furthermore, 2D projection effects may be largely responsible for particle centre-to-centre distances that are smaller than the diameter of individual SPIONS.

The presence of a magnetic field likely played a strong role in aggregate formation. It has been established that field-induced increases in SPION magnetic moment strength and

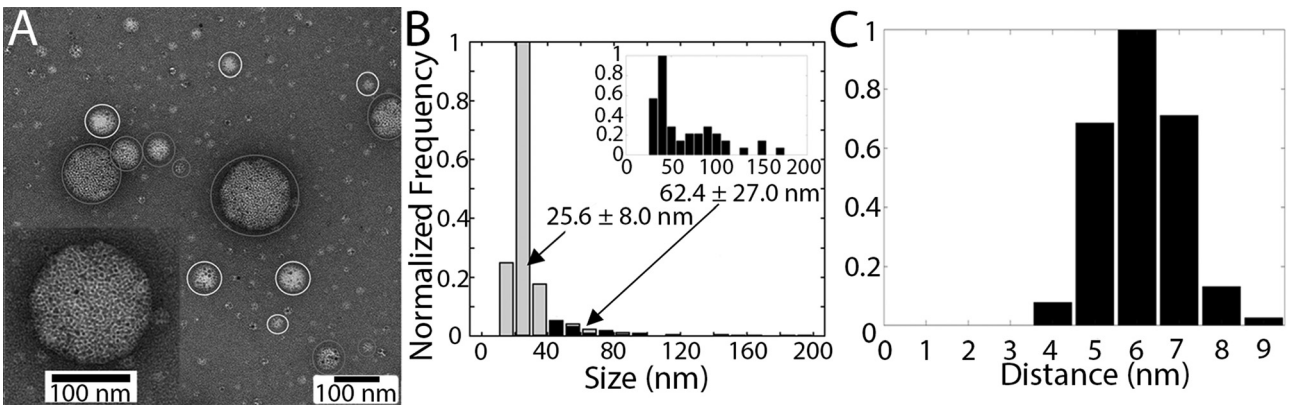

Fig. 2 (A) TEM of nanocomposites produced at a SPION: polymer mole ratio = 1 in the absence of an applied magnetic field indicates three distinct populations: densely loaded aggregates (grey circles), SPION-micelles (white circles), and empty micelles (small white spheres in background). Inset: Magnified image of a densely loaded aggregate indicating some internal ordering (*i.e.*, chaining) and tightly packed NP distribution, (B) size distribution of the SPION nanocomposites synthesized in the absence of magnetic field (grey: entire population, black: densely loaded aggregates only). Inset: log-normal size distribution for densely loaded aggregates, (C) the interparticle distances, *d*, for SPIONs encapsulated in densely loaded aggregates synthesized in the absence of a magnetic field. The distribution has been normalized by the mode and presented as normalized frequency. The average value for the 100 measurements made was $d = 5.6 \pm 0.94$ nm.

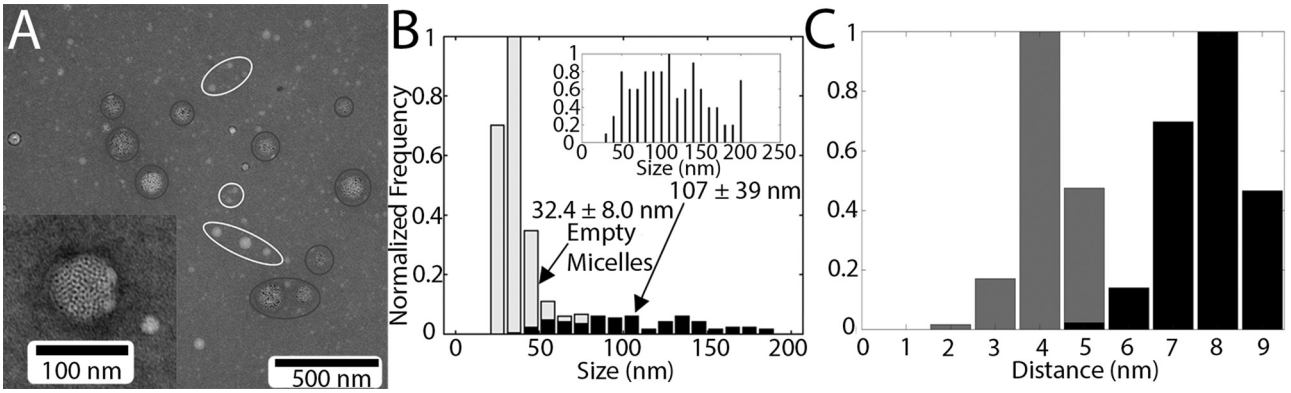

Fig. 3 (A) TEM of nanocomposites produced at a SPION: polymer mole ratio = 1 in the presence of a magnetic field shows two populations: densely loaded aggregates (grey circles) and empty micelles (white circles). Inset: Magnified image of a densely loaded aggregate shows SPIONs are tightly packed and are locally arranged in arrays, (B) size distribution of SPION nanocomposites synthesized in the presence of a magnetic field (grey: entire population, black: densely loaded aggregates only). Inset: Densely loaded aggregates synthesized in the presence of a magnetic field appear to follow Gaussian size distribution, (C) there are two characteristic interparticle distances for SPIONs in densely loaded aggregates synthesized in the presence of a magnetic field. The grey bars correspond to the distances between particles within a particle chain. The black bars correspond to the distances between particles in adjacent particle chains. Disordered particles were not considered in these measurements. Both distributions have been normalized to their respective modes. The average value for the 100 measurements made was d = 3.72 ± 0.61 nm and 7.28 ± 0.81 nm, respectively.

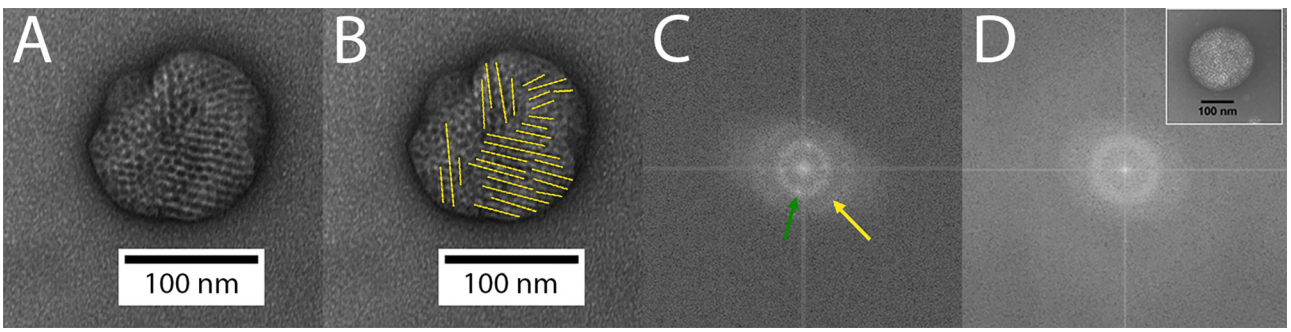

Fig. 4 (A) TEM images of an example a SNC-St, with (B) increased ordering indicated by the formation of periodic linear arrays (yellow lines), (C) fast Fourier transform (FFT) of (A). The diffraction spots (green arrow) and outer elliptical halo indicating directional semi-periodicity (yellow) in the FFT are consistent with reports of short range order,[1] (D) FFT of a SNC shown in Fig. 2. No diffraction spots are observed in these samples.

alignment can trigger the formation of uniformly sized, linearly aligned SPION arrays.[31] During aggregation, SPIONs will spontaneously align their easy axes to minimize their free energy by dipole coupling. These SPION arrays may then form densely loaded aggregate through nucleation and growth mechanisms. SPION arrays interact *via* strong dipole–dipole interactions that are stronger than those of SPIONs not exposed to a magnetic field. Array aggregation will depend on the competition between dipole coupling within the existing aggregate and that with the incoming SPION array, as aggregates will attempt to minimize their overall free energy. To integrate a new SPION array into the aggregate, SPIONs must either internally realign their magnetic dipoles or physically arrange the incoming array to minimize the resulting free energy. Beyond a limiting size, strong internal dipole coupling within the existing densely loaded aggregate may repel addition of new SPION arrays. Additionally, steric limitations for SPION arrays magnetic field much higher than those for individual SPIONs. Thus, the shift from log normal to Gaussian size distribution and the increase in ordering in the presence of magnetic fields observed in densely loaded aggregates may result from SPION arrays comprised of individual SPIONs aligning their magnetization with the rotating magnetic field of the stir bar against thermal fluctuations.

In addition to the application of a magnetic field during synthesis, emulsion solutions also experienced increased and longer mixing during the solvent evaporation phase resulting from magnetic stirring compared to solutions that were left on a rocker during the solvent evaporation phase. This may have resulted in changes in emulsion droplet size, solvent evaporation rates, and solvent concentration profiles. For example, faster solvent evaporation should increase the formation of non-equilibrium structures as a result of kinetic trapping.

Thus, magnetic forces combined with enhanced mixing likely account for the statistically significant size increase observed in the densely loaded aggregates associated with SNC-Sts *vs.* SNCs, as aggregate growth is stabilized against thermal fluctuations by magnetic forces. This phenomenon

has been previously observed in solution[32] in the absence of BCPs and may be augmented by short-range, attractive van der Waals forces between NPs. Thus, the combination of the attractive magnetic and van der Waals forces, aided by the presence of BCP that serves as an entropic barrier to reconfiguration, likely stabilizes semi-ordered NP aggregates so that structure is maintained even after the external magnetic field is removed. In these structures the BCP may intercalate between linear arrays as well as coating the surface of the aggregate and intercalating within the first few NP layers. The preserved internal structuring observed here is highly desirable because increased ordering can lead to enhanced magnetism.[31]

Effect of magnetic field exposure after SPION aggregate synthesis

To determine whether transformation to more ordered structures can be induced post-synthesis, we exposed SNCs synthesized in the absence of an external field to a permanent magnet field ($0 \leq$ magnetic field (Oe) ≤ 5000) (Fig. S3, ESI‡). Samples in test tubes were placed on the surface of a permanent magnet for 9 hours, giving rise to two experimental populations: a sample of composites that accumulated near the magnet surface (*i.e.*, SNC-P) and composites remaining in the supernatant (*i.e.*, SNC-S) (Fig. 5). Because the magnetic field declines as $1/d^3$ (where d = separation distance),[12] it is possible that particles in the supernatant included larger aggregates that did not diffuse sufficiently close enough to the magnet to be trapped or aggregates less enriched in SPIONs, *i.e.*, empty micelles, SPION-micelles with inherently lower loading, or less densely loaded aggregates.[21]

The percent of densely loaded aggregates and micelles (*i.e.*, empty or SPION) and their sizes were quantified in both SNC-P and SNC-S samples (Table 1). The percentage of densely loaded aggregates in the SNC-P sample increased (39.5%) after magnetic exposure relative to the population prior to magnetic exposure (8.5%) and the population in the SNC-S sample (8.1%). With post-synthesis magnetic field exposure, densely loaded aggregates displayed log normal size distributions with mean sizes of $\sim 50.2 \pm 21.0$ nm and $\sim 54.6 \pm 22.0$ nm for the SNC-P and SNC-S samples, respectively (Table 1). There was no statistically significant difference in mean densely packed aggregate size (significance level of $\alpha = 0.05$) between the SNC-P, SNC-S, and SNC samples. Furthermore, there was no obvious difference in SPION arrangement within the densely loaded structures in either magnetically treated sample relative to the control. Thus, although magnetic field exposure post-synthesis enriched the pellet with densely loaded aggregates, it did not change mean size or visible internal ordering, unlike magnetic field exposure during synthesis. As these structures are derived from SNC samples not exposed to fields, BCP arrangement is expected to be similar with hydrophobic chains interacting with the NP aggregate surface and possible intercalating with selected NPs. Structures that appeared to have 'fused' *via* polymer bridges were occasionally seen in the SNC-P samples, but not in control samples (Fig. S4 and S5, Supplemental Results and discussion, ESI‡). Further investigation necessary to determine the origin of these fused structures is beyond the scope of this investigation.

The accumulation of more densely loaded aggregates in SNC-P is consistent with the larger magnetic force experienced by these nanocomposites compared to the smaller, individual SPIONs or SPION micelles and the higher diffusivity of the latter relative to the former. Previously, we have shown that magnetic forces on the order of 0.1–0.2 pN are required to capture similar nanocomposites[33,34] and that neodymium magnets can capture particles within ~ 2 μm of their surfaces.[35] The absence of significant size change in the pellet or supernatant can be explained by structure stabilization engendered by strong van der Waals forces, dipole–dipole interactions between SPIONs, and entropic stabilization provided by the BCPs. These results indicate that magnetic forces applied after composite formation were not sufficient to break BCP entropic barriers to change composite size, at least at the strengths investigated here. Based on the test tube thickness and the magnet employed, exposure resulted in a magnetic field gradient of $2000 \leq$ magnetic field (Oe) ≤ 5000 across the entire sample (Fig. S3, ESI‡), which would vary in the z dimension during composite diffusion. Although the densely loaded aggregate population in the SNC-P sample was enriched, the lack of complete removal of densely loaded aggregates from the SNC-S most likely resulted from field variation in the z dimension. Additional research is needed to optimize the magnetic field gradient, exposure time, and sample orientation for more efficient size-based magnetic concentration.

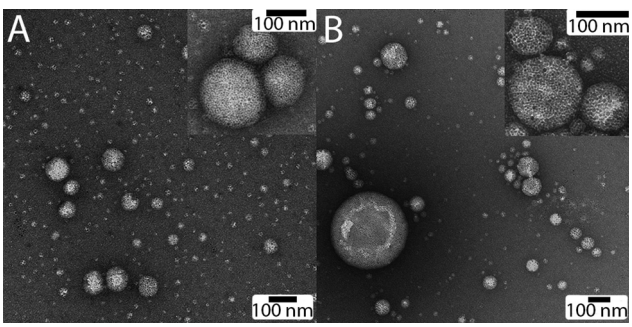

Fig. 5 TEM of nanocomposites produced at a SPION: polymer mole ratio = 1 in the absence of an applied magnetic field then separated magnetically into (A) SNC-P and (B) SNC-S samples. Insets: Magnified images of densely loaded aggregates show limited internal ordering (*i.e.*, chaining) and tightly packed NPs.

Effect of magnetic field exposure on SPION ordering and spacing[36]

To confirm the impact of external magnetic fields on inter-SPION distance and organization in densely loaded SPION-PS-*b*-PEO aggregates, small angle X-ray scattering (SAXS) experiments were performed. The spectra measured for SNC-St samples were compared to those measured for SNC, SNC-P, and SNC-S samples (Fig. 6). As in our earlier work, the spectra have a strong feature near $q \sim 1.1$ nm^{-1} – in this case a rather sharp peak – that arises from the arrangement of the closely-packed,

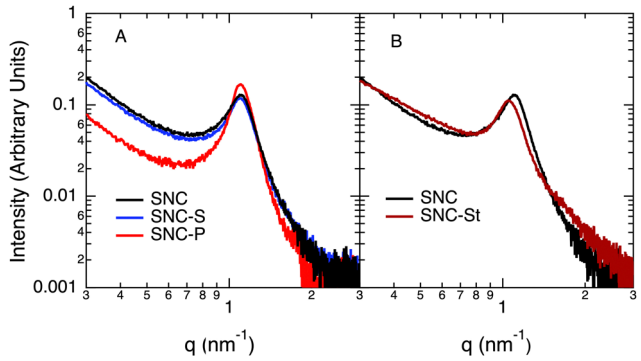

Fig. 6 (A) SAXS spectra of SPION aggregates stabilized by PS-*b*-PEO and produced in the absence of a magnetic field: SNC (black), SNC-P (red) and SNC-S (blue) after post-synthesis exposure to a magnet. (B) SAXS spectra of SPION aggregates stabilized by PS-PEO and produced either in the absence (SNC, black) or presence (SNC-St, red) of a magnetic field.

~5 nm particles within the densely loaded aggregates. The increasing intensity at lower q is associated with scattering from the empty micelles, SPION micelles, and the aggregates themselves.

All samples made in the absence of a magnetic field display a peak at the same location, q = 1.10 Å^{-1}, irrespective of whether they were exposed to a magnetic field post-synthesis. This value of q corresponds to a characteristic spacing $d = 2\pi/q$ = 5.7 nm. Complementary TEM results yield an average interparticle spacing of 5.61 ± 0.94 nm for these samples. The latter value is in good agreement with the SAXS value. The full width at half max (FWHM) of these peaks are all close to ~0.11 nm^{-1}, suggesting the interparticle distance does not vary significantly in the particles that contribute to this peak. SPIONs are coated with an oleic acid capping ligand with a molecular size of ~2 nm, thus nanoparticles are likely not directly touching in these samples.

In contrast, the SNC-St samples produced in the presence of the magnetic field show a peak at a slightly lower value q = 1.05 nm^{-1}, corresponding to d = 5.98 nm. The full width at half max of these peaks is ~0.10 nm^{-1}. The increase in distance observed in SAXS is consistent with the presence of a longer spacing length scale observed between the adjacent chains of aligned particles. Given the broad distribution of particle spacings (Fig. 3C) and the presence of less well-organized particles within the aggregates; however, it is not surprising that we do not see two peaks – one corresponding to each interparticle spacing observed in TEM. Finally, the SAXS results confirm that the TEM images are representative of the aggregates throughout the solution.

Effect of external magnetic fields on magnetic nanocomposites

To establish structure–property relationships between SPION aggregates with and without magnetic field exposure, magnetization was studied as a function of temperature (zero field cooled (ZFC) and field cooled (FC) curves) and externally applied magnetic field (−10 kOe to +10 kOe) at temperatures of 300 K and 5 K in a SQUID magnetometer. The magnetic behaviour of non-interacting SPIONs in zero applied field is determined by the competition between two energy scales: the anisotropy energy associated with the effective anisotropy field, H_{eff}, arising from a combination of shape anisotropy and crystal-field (or spin–orbit) interactions within the SPION, and thermal energy, k_BT. When the anisotropy energy, given by $E_a = mH_{eff}$ (where m is the magnetization of the SPION), is much less than k_BT, the magnetization of an individual SPION fluctuates randomly in space, mimicking the behaviour of a paramagnetic spin. This is typically referred to as the superparamagnetic regime. As temperature decreases, however, E_a will dominate, freezing the SPION magnetization into an orientation determined by the magnetic anisotropy. This low temperature regime is often referred to as the "ferromagnetic" phase in the literature, and the transition temperature between these two regimes, where $E_a = k_BT$, is known as the blocking temperature,[37] T_B. The coercive field (H_C) required to unblock the thermally trapped SPIONs also depends on the temperature in the same manner. We note that this low temperature regime is distinct from the ferromagnetic phase transition governing the magnetic ordering of spins within the SPION nanoparticle that give rise to its overall magnetic moment, which is typically over 500 °C.[38]

However, when analysing SPIONs in close proximity, such as in densely loaded aggregates, dipole–dipole interactions (E_{dd}) become relevant. As a result, T_B is proportional to an additive function of E_a and E_{dd}, and H_C is also altered.[39] These dipole interactions can align head-to-tail in-line or in vertical ferromagnetic (parallel) or anti-ferromagnetic (antiparallel) arrangements (Fig. 7). Effective E_{dd} decreases (and free energy increases) in the order of head-to-tail in-line > antiferromagnetic > ferromagnetic orientation. Thus, head-to-tail in-line orientation is energetically most-favoured during SPION assembly in 1D, and results in the highest T_B. Similarly, effective E_a and therefore H_C for in-line or ferromagnetic orientations is higher than that of antiferromagnetic orientations. However, in a 3D cluster of SPIONs, this relationship is much more complex. Similar to T_B, H_C of the interacting system is also influenced by the dipole coupling between SPIONs and depends on the dipole-coupled shape anisotropy and volume.[31] Thus, measurements of T_B and H_C can provide critical information on the structure of magnetic field treated and untreated densely loaded aggregates present in the SNCs, as well as insights into their structure–property relationships.

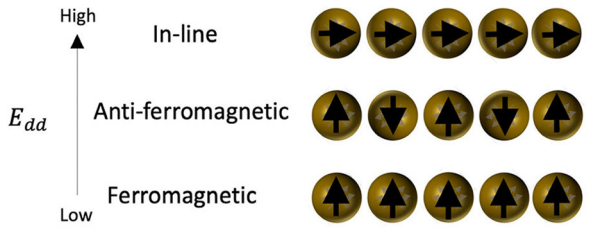

Fig. 7 SPION dipole–dipole coupling arrangements available in 1D.

Table 2 Blocking temperature (T_B) and coercivity (H_C) of dispersed SPIONs and densely loaded aggregates in the presence and absence of a magnetic field[a]

Sample	T_B (K)	H_C (Oe)
Dispersed, individual SPIONs	8	50
SNC	16	67
SNC-St	20	78
SNC-P	24	50
SNC-S	16	67

[a] Normalized standard deviation of magnetic measurement fits are reported in Table S1 (ESI).

We investigated the difference in magnetic properties of dispersed SPIONs and SNC, SNC-St, SNC-P, and SNC-S samples (Table 2 and Fig. S6–S11, ESI‡). Individual SPIONs were dispersed in a PMMA matrix to prevent interactions during testing. Dispersed SPIONs lack ordering and have the lowest T_B. The SNC samples have increased ordering and dipole–dipole interactions, and thus have a T_B double that of dispersed SPIONs. SNC-St and SNC-P samples follow the same trend of increased T_B with increased ordering. Interestingly, this trend is not observed in the SNC-S sample, which exhibits the same T_B as the SNC sample. The differences in H_C are too small to reveal statistically significant structural/magnetic insight for all the samples.

Effect of magnetic field exposure on polymer properties

SQUID results suggest increased magnetism and dipole coupling for samples exposed to magnetic fields either during or post synthesis. Such dipole coupling has the potential to disrupt polymer chain interactions, especially of glassy PS blocks in the BCP. Stronger dipole coupling, such as that observed in more aligned samples like the SNC-St, should exert greater disruption on polymer networks and therefore the glass transition temperature (T_g). Thus, to evaluate the potential influence of dipole coupling on polymer properties, we examined the T_g of SNCs formed in the presence and absence of fields and exposed to fields post-synthesis (Fig. 8 and Fig. S12, ESI‡). All differential scanning calorimetry (DSC) thermograms collected showed no evidence of hysteresis between replicate runs, suggesting that the transitions are both reversible and repeatable.

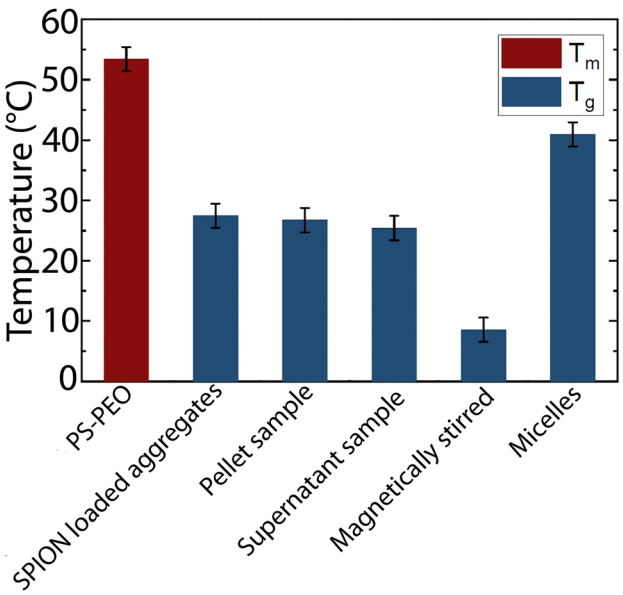

Fig. 8 Melting (T_m) and glass transition (T_g) temperatures for pure PS-PEO polymer, SNC, SNC-P, SNC-S, SNC-St samples, and PS-PEO micelles.

Pure PS-PEO polymer examined as a control exhibited a melting transition at 53.4 °C, which was not observed in any of the SNC samples tested. SPION nanocomposites yielded glass transitions even with relatively slow rates of cooling, suggesting easy supercooling. The SNC sample displayed a T_g of 27.4 °C, whereas the SNC-P and SNC-S samples show T_g values of 27.4 and 26.7 °C, respectively. Since these values are largely unchanged from the SNC sample, it is likely that magnetic exposure post-synthesis does not produce a systematic change in polymer chain interactions. The SNC-St sample exhibited a T_g of 8.6 °C, a marked decrease of nearly 20 degrees from the other SNC samples investigated. Glass transitions are directly dependent on dynamic intermolecular forces, so a sharp decrease in T_g suggests that changes introduced into the structure of SNC-St either reduce the overall intermolecular force strength or increase the free volume of the system. Increased ordering seen in TEM can cause a decrease van der Waals forces, leading to the noticeable decrease in T_g. Similarly, when a sample of pure micelle structures with no SPIONs is tested, there is an increase in T_g (up to 40.9 °C) suggesting the opposite is happening. This is likely results from the lack of SPION encapsulation changing the packing and volume fractions. The observation of a single T_g suggests that the BCPs behave as statistical polymers in this confinement regime. If the different polymer domains were still distinct, we would expect the T_g to be around −55 °C (Lindeman's criterion verified by experiments of confined PEO, *e.g.*, in ref. 40), which is not the case. These data suggest the possibility of single chain confinement between nanoparticles and nanoparticle arrays.

Conclusions

This work examines the role of magnetic field on ordering, magnetic properties, and structural properties of polymer stabilized SPION aggregates synthesized by the interfacial instability method. Magnetic field application was shown to induce magnetic ordering and structural changes through a combination of TEM, SAXS, SQUID, and DSC measurements. Specifically, semi-periodic ordering of SPIONs with transformation to larger aggregate sizes, higher magnetic response, and lower T_g was observed in SNC-St samples, whereas magnetic response enhancement with undetectable structural change was observed in SNC-P samples. These data show that magnetic field application can alter the magnetic properties of the aggregate, which could directly impact their efficacy in magnetic cell sorting

or magnetic resonance imaging applications. Additionally, our T_g observations combined with SAXS data suggest that BCP blocks are confined between NPs and NP arrays, behaving as statistical polymers, which may afford opportunities to study and alter single chain dynamics.

Although modifications in morphology and structure have previously been achieved by changing reaction conditions, such as using different stabilizing polymer compositions[21] or concentrations,[23] these methods are severely limited in controlling magnetic order in colloidal SPION aggregates. The use of magnetic fields provides a unique opportunity to manipulate magnetic structure, in addition to physical structure, of densely loaded aggregates that could potentially be applied to composites of differing composition. Further, diverse structural and magnetic modifications can be achieved, depending on the timing of magnetic field application (*i.e.*, during or after synthesis), enabling experimental exploration of superferromagnetic and spin-glass phases of SPION assemblies. As a result, this technique offers enhanced capability to tailor 3D SPION aggregate structure and properties, by employing inherent properties of SPION constituents. As such, this approach could enable SPION aggregates to be harnessed for applications in targeted hyperthermia, separations, magnetic resonance imaging, or photonics.

Author contributions

The manuscript was written and edited by all of the authors. All authors have given approval to the final version of the manuscript. GMN and AVD contributed equally to this work. GMN, AVD, and EJ synthesized and characterized particles sizes under the guidance of JOW. BEW performed SAXS experiments and analysis. AVD conducted SQUID measurements under the guidance of EJH. EJ and BBH conducted DSC measurements under the guidance of JS. MS modelled the theoretical aspect of SPION assembly. JOW, BEW, JS, and EJH designed and conceived experiments.

Conflicts of interest

There are no conflicts to declare.

Acknowledgements

This work was funded by the NSF under grants DMR-1206745, DMR-2011876 (particle synthesis) and DMR-1420451 (characterization). Funding for this research was provided by the Center for Emergent Materials: an NSF MRSEC under award number DMR-2011876. This research used resources of the Advanced Photon Source, a U.S. Department of Energy (DOE) Office of Science User Facility operated for the DOE Office of Science by Argonne National Laboratory under Contract No. DE-AC02-06CH11357. We thank S. Siefert and R. Winans for their help with the SAXS experiments.

Notes and references

1 S. J. Yoo, C. Y. Kim, J. W. Shin, S. G. Lee, J. M. Jeong, Y. J. Kim, S. H. Lee and J. G. Kim, *Mater. Charact.*, 2013, **78**, 31–36.
2 Z. H. Nie, A. Petukhova and E. Kumacheva, *Nat. Nanotechnol.*, 2010, **5**, 15–25.
3 L. G. Xu, W. Ma, L. B. Wang, C. L. Xu, H. Kuang and N. A. Kotov, *Chem. Soc. Rev.*, 2013, **42**, 3114–3126.
4 Z. D. Lu and Y. D. Yin, *Chem. Soc. Rev.*, 2012, **41**, 6874–6887.
5 T. Wang, D. LaMontagne, J. Lynch, J. Q. Zhuang and Y. C. Cao, *Chem. Soc. Rev.*, 2013, **42**, 2804–2823.
6 M. P. Pileni, *J. Phys. Chem. B*, 2001, **105**, 3358–3371.
7 B. L. V. Prasad, C. M. Sorensen and K. J. Klabunde, *Chem. Soc. Rev.*, 2008, **37**, 1871–1883.
8 B. Auguie and W. L. Barnes, *Phys. Rev. Lett.*, 2008, **101**, 4.
9 D. Vanmaekelbergh, *Nano Today*, 2011, **6**, 419–437.
10 N. Vogel, M. Retsch, C. A. Fustin, A. del Campo and U. Jonas, *Chem. Rev.*, 2015, **115**, 6265–6311.
11 M. A. Boles, M. Engel and D. V. Talapin, *Chem. Rev.*, 2016, **116**, 11220–11289.
12 S. Singamaneni, V. N. Bliznyuk, C. Binek and E. Y. Tsymbal, *J. Mater. Chem.*, 2011, **21**, 16819–16845.
13 R. A. Ortega and T. D. Giorgio, *J. Nanopart. Res.*, 2012, **14**, 1282.
14 J. A. Johnson, A. Dehankar, A. Robbins, P. Kabtiyal, E. Jergens, K. Ho Lee, E. Johnston-Halperin, M. Poirier, C. E. Castro and J. O. Winter, *Mater. Sci. Eng., R*, 2019, **138**, 153–209.
15 Y. Tian, J. R. Lhermitte, L. Bai, T. Vo, H. L. Xin, H. Li, R. Li, M. Fukuto, K. G. Yager, J. S. Kahn, Y. Xiong, B. Minevich, S. K. Kumar and O. Gang, *Nat. Mater.*, 2020, **19**, 789–796.
16 F. Hong, F. Zhang, Y. Liu and H. Yan, *Chem. Rev.*, 2017, **117**, 12584–12640.
17 Q. J. Luo, R. J. Hickey and S. J. Park, *ACS Macro Lett.*, 2013, **2**, 107–111.
18 B. Kiani, D. Faivre and S. Klumpp, *PLoS One*, 2018, **13**, e0190265.
19 D. Wang, B. B. Lin, T. P. Shen, J. Wu, F. H. Hao, C. C. Xia, Q. Y. Gong, H. R. Tang, B. Song and H. Ai, *Chin. Phys. B*, 2016, **25**, 077504.
20 L. Lartigue, P. Hugounenq, D. Alloyeau, S. P. Clarke, M. Levy, J. C. Bacri, R. Bazzi, D. F. Brougham, C. Wilhelm and F. Gazeau, *ACS Nano*, 2012, **6**, 10935–10949.
21 P. H. Qiu, C. Jensen, N. Charity, R. Towner and C. B. Mao, *J. Am. Chem. Soc.*, 2010, **132**, 17724–17732.
22 C. Schmidtke, R. Eggers, R. Zierold, A. Feld, H. Kloust, C. Wolter, J. Ostermann, J. P. Merkl, T. Schotten, K. Nielsch and H. Weller, *Langmuir*, 2014, **30**, 11190–11196.
23 G. M. Nabar, J. O. Winter and B. E. Wyslouzil, *Soft Matter*, 2018, **14**, 3324–3335.
24 J. Xu, K. Mahajan, W. Xue, J. O. Winter, M. Zborowski and J. J. Chalmers, *J. Magn. Magn. Mater.*, 2012, **324**, 4189–4199.
25 J. T. Zhu and R. C. Hayward, *J. Am. Chem. Soc.*, 2008, **130**, 7496–7502.
26 J. Bae, J. Lawrence, C. Miesch, A. Ribbe, W. K. Li, T. Emrick, J. T. Zhu and R. C. Hayward, *Adv. Mater.*, 2012, **24**, 2735–2741.

27 C. A. Schneider, W. S. Rasband and K. W. Eliceiri, *Nat. Methods*, 2012, **9**, 671–675.
28 K. H. Lee, G. Yang, B. E. Wyslouzil and J. O. Winter, *ACS Appl. Polym. Mater.*, 2019, **1**, 691–700.
29 K. Ho Lee, M. Ireland, B. L. Miller, B. E. Wyslouzil and J. O. Winter, *J. Colloid Interface Sci.*, 2021, **586**, 445–456.
30 A. Jada, G. Hurtrez, B. Siffert and G. Riess, *Macromol. Chem. Phys.*, 1996, **197**, 3697–3710.
31 C. P. Jiang, C. W. Leung and P. W. T. Pong, *Nanoscale Res. Lett.*, 2016, **11**, 12.
32 M. J. Park, J. Park, T. Hyeon and K. Char, *J. Polym. Sci., Part B: Polym. Phys.*, 2006, **44**, 3571–3579.
33 G. Ruan, G. Vieira, T. Henighan, A. R. Chen, D. Thakur, R. Sooryakumar and J. O. Winter, *Nano Lett.*, 2010, **10**, 2220–2224.
34 K. D. Mahajan, G. Ruan, C. J. Dorcena, G. Vieira, G. Nabar, N. F. Bouxsein, J. J. Chalmers, G. D. Bachand, R. Sooryakumar and J. O. Winter, *Nanoscale*, 2016, **8**, 8641–8649.
35 K. D. Mahajan, Y. Cui, C. J. Dorcéna, N. F. Bouxsien, G. D. Bachand, J. J. Chalmers and J. O. Winter, *Biotechnol. J.*, 2018, **13**, 1700402.
36 G. M. Nabar, PhD thesis, The Ohio State University, 2017.
37 G. Kandasamy and D. Maity, *Int. J. Pharm.*, 2015, **496**, 191–218.
38 A. S. Teja and P.-Y. Koh, *Prog. Cryst. Growth Charact. Mater.*, 2009, **55**, 22–45.
39 V. Schaller, G. Wahnstrom, A. Sanz-Velasco, P. Enoksson and C. Johansson, *J. Magn. Magn. Mater.*, 2009, **321**, 1400–1403.
40 T. Uemura, N. Yanai, S. Watanabe, H. Tanaka, R. Numaguchi, M. T. Miyahara, Y. Ohta, M. Nagaoka and S. Kitagawa, *Nat. Commun.*, 2010, **1**, 83.